Eur. Phys. J. Plus (2019) **134**: 233
DOI 10.1140/epjp/i2019-12543-0

THE EUROPEAN PHYSICAL JOURNAL PLUS

Regular Article

Wave propagation in functionally graded cylindrical nanoshells based on nonlocal Flügge shell theory

Yan Qing Wang[1,2,a], Chen Liang[1], and Jean W. Zu[3]

[1] Department of Mechanics, College of Sciences, Northeastern University, Shenyang 110819, China
[2] Key Laboratory of Ministry of Education on Safe Mining of Deep Metal Mines, Northeastern University, Shenyang 110819, China
[3] Schaefer School of Engineering and Science, Stevens Institute of Technology, Hoboken NJ 07030, USA

Received: 29 October 2018 / Revised: 15 January 2019
Published online: 27 May 2019

Abstract. In the present work, wave propagation characteristics of circular cylindrical nanoshells made of functionally graded materials are investigated. Material properties of the nanoshells are graded in the thickness direction according to the power-law distribution. The Flügge shell theory together with the nonlocal elasticity theory is employed to model the present system. The wave dispersion relations with respect to the wave number in the longitudinal and circumferential directions are derived. In addition, a parametric study is carried out to highlight the influences of the power-law exponent, the wave number, the nonlocal parameter and the radius-to-thickness ratio. The results indicate that these parameters have a significant effect on the wave propagation characteristics of functionally graded material (FGM) cylindrical nanoshells.

1 Introduction

Since the concept of functionally graded materials (FGMs) was first proposed by Japanese material scientists in 1984 [1], this type of materials has attracted extensive attention from research and engineering communities [2–8]. FGMs are inhomogeneous composite materials made of two or more materials, in which the material properties exhibit a graded variation from one surface to the other. Such unique design can impart the mechanical properties of component materials to the integrations. For example, FGMs typically containing the specific metallic and ceramic constituents have the advantages of both materials. On the one hand, the ceramic constituent, owing to its low thermoconductivity, supplies high temperature resistance; on the other hand, the metal component provides good toughness and ductility which can prevent fracture [9].

Due to their excellent designability and mechanical property, FGMs have shown immense potential and application future in shape memory alloys [10], and microelectromechanical systems (MEMS) and nanoelectromechanical systems (NEMS) [11–13]. For instance, the FGM shape memory alloy micro/nano-films with new surface properties, namely, wear, corrosion resistant and biocompatibility, can fulfill the tribological and orthodontic applications [14]. The double-sided FGM nanobridges are regarded as very good candidates for miniature electrodes in NEMS [15]. FGM poly-SiGe multilayers were proposed as a promising MEMS device for the integrated circuit [16]. FGM poly-SiGe electrodes could be applied to the fabrication of monolithic integration [17].

FGM cylindrical nanoshells are prevalent FGM nanostructures in practical engineering applications. Therefore, the mechanical properties of FGM cylindrical nanoshells have attracted a sight of interests. Using the first-order shear deformation (FSD) theory, Arefi and Zenkour [18] presented a two-dimensional thermoelastic analysis of FGM cylindrical nanoshells via the nonlocal elasticity theory. Mohammadi *et al.* [19] investigated the vibrational behavior of FGM cylindrical nanoshells with the consideration of simply supported and clamped-clamped boundary conditions. Zhu *et al.* [20] studied the effect of surface energy on the torsional buckling behavior of FGM cylindrical nanoshells covered with piezoelectric nanolayers. Sahmani and Aghdam [21] dealt with the nonlinear instability of FG multilayer graphene platelet-reinforced nanoshells under axially compressive load by using the nonlocal strain gradient theory. Based on the hyperbolic shear deformation shell theory, Sahmani and Aghdam [22] carried out the radial postbuckling analysis

[a] e-mail: wangyanqing@mail.neu.edu.cn

of FG multilayer graphene platelet-reinforced nanoshells subjected to hydrostatic pressure including nonlocal elastic and strain gradient stress fields. Sun *et al.* [23] presented analytical solutions for the buckling of carbon nanotubes and FGM cylindrical nanoshells under compressive and thermal loads via Reddy's higher-order shear deformation theory. Using the generalized differential quadrature method to obtain the governing equations associated with boundary conditions, Shojaeefard *et al.* [24] investigated the buckling and vibration of FGM piezomagnetic nanoshells embedded in viscoelastic media. Zeighampour and Shojaeian [25] studied vibration of FGM sandwich cylindrical nanoshells by employing the FSD theory and the couple stress theory. Fang *et al.* [26] carried out the nonlinear buckling and postbuckling analyses of FGM piezoelectric cylindrical nanoshells with the consideration of surface energy effect.

It should be noted that the wave propagation characteristics of nanoscale shells has been one of the most interesting research topics in academic and industrial groups. Hu *et al.* [27] performed the torsional and transverse wave propagation analysis of single- and double-walled carbon nanotubes; they found that the results of the nonlocal cylindrical shell theory have good agreement with those of molecular dynamics simulations. On the basis of the nonlocal strain gradient theory, Zeighampour *et al.* [28] investigated the wave propagation in fluid-conveying double-walled carbon nanotubes. Later, Zeighampour *et al.* [29] utilized the nonlocal strain gradient theory to study the wave propagation in viscoelastic thin cylindrical nanoshells resting on a visco-Pasternak foundation. The wave propagation characteristics of magneto-electro-elastic nanoshells was studied in the work of Ma *et al.* [30] by using the nonlocal strain gradient theory, where the Kirchhoff-Love and first-order shear deformation shell models were employed. Considering the small-scale effect, Wang and Varadan [31] investigated the wave propagation characteristics of carbon nanotubes on the basis of Eringen's nonlocal elasticity theory.

A literature survey shows that no study has been conducted on wave propagation characteristics in nanoscale shells made of FGMs. In this context, the present paper aims to give an analytical study on this problem. The Flügge shell theory in conjuction with the nonlocal elasticity theory is employed for deriving the theoretical formulations of the present model. Additionally, the wave propagation characteristics of FGM cylindrical nanoshells under various system parameters are shown in detail.

2 Material properties of FGM circular cylindrical nanoshells

For FGM nanoshells, material properties P_i of constituent materials are functions of temperature [32]:

$$P_i = P_0\left(P_{-1}T^{-1} + 1 + P_1T + P_2T^2 + P_3T^3\right), \tag{1}$$

where T is the Kelvin temperature; P_{-1}, P_0, P_1, P_2 and P_3 are the temperature coefficients and unique to the constituent materials.

The general material properties P of FGMs are determined by individual material properties P_i and volume fractions V_{fi} of the constituent materials [3]:

$$P = \sum_{i=1}^{N} P_i V_{fi}. \tag{2}$$

The summation of volume fractions of all the constituent materials should be one, namely,

$$\sum_{i=1}^{N} V_{fi} = 1. \tag{3}$$

For a cylindrical nanoshell with the uniform thickness h, suppose that the reference surface is at the middle surface; hence, the volume fraction is [4,33]

$$V_f = \left(\frac{z}{h} + \frac{1}{2}\right)^p, \tag{4}$$

where p $(0 \le p < \infty)$ is the power-law exponent; z $(-h/2 \le z \le h/2)$ is the radial distance from the middle surface in the thickness direction.

Suppose that an FGM circular cylindrical nanoshell is made of metal (nickel) and ceramic (Al_2O_3); and the inner and outer surfaces are pure metal and pure ceramic, respectively. Based on the rule of mixture, Young's modulus $E(z)$, mass density $\rho(z)$, and Poisson's ratio $\mu(z)$ of the FGM nanoshell can be described as [34]

$$E(z) = (E_c - E_{ni})\left(\frac{z}{h} + \frac{1}{2}\right)^p + E_{ni}, \tag{5}$$

$$\rho(z) = (\rho_c - \rho_{ni})\left(\frac{z}{h} + \frac{1}{2}\right)^p + \rho_{ni}, \tag{6}$$

$$\mu(z) = (\mu_c - \mu_{ni})\left(\frac{z}{h} + \frac{1}{2}\right)^p + \mu_{ni}. \tag{7}$$

Clearly, when $z = -h/2$, the general material properties correspond to those of pure nickel, *i.e.*, $E(z) = E_{ni}$, $\rho(z) = \rho_{ni}$, and $\mu(z) = \mu_{ni}$; when $z = h/2$, the general material properties correspond to those of pure ceramic, namely, $E(z) = E_c$, $\rho(z) = \rho_c$, and $\mu(z) = \mu_c$.

3 Nonlocal continuum model of FGM circular cylindrical nanoshells

The theory of nonlocal elasticity [35] assumes that the stresses at reference point x is a function of the strain field at every point in the body. The most general form of the constitutive relation in the nonlocal elasticity relates to the integral over the entire area. The integral contains a nonlocal kernel function, which describes the corresponding effects of the strains at different locations on the stresses at a given location.

The constitutive relationships for nonlocal elasticity are given by [36]

$$\sigma_{ij,j} = 0, \tag{8}$$

$$\sigma_{ij}(x) = \int_V \alpha(|x - x'|, \tau)\sigma_{ij}^c(x')\,\mathrm{d}V(x'), \tag{9}$$

$$\sigma_{ij}^c(x') = C_{ijkl}\varepsilon_{kl}(x'), \tag{10}$$

$$\varepsilon_{ij} = \frac{1}{2}(u_{i,j} + u_{j,i}), \tag{11}$$

in which σ_{ij}, ε_{ij} and u_i are stress tensor, strain tensor and displacement vector, respectively; $\sigma_{ij}^c(x')$ and C_{ijkl} are the classical stress tensor and elastic modulus tensor in classical elasticity, respectively; $\alpha(|x - x'|, \tau)$ is a nonlocal modulus or attenuation function, which incorporates the nonlocal effects at the reference point x that are produced by local strain at the source x' into the constitutive relations. $|x - x'|$ is Euclidean distance; $\tau = e_0 a/l$ [35], where e_0 is a constant corresponding to each material, a is an internal characteristic length and l is an external characteristic length. The value of e_0 needs to be determined experimentally or by matching the dispersion curves of plane waves with those of atomic lattice dynamics.

The integral-partial differential equations of the above linear nonlocal elasticity are reduced to singular partial differential equations of a special class of physically admissible kernel [36]. So, Hook's law for the stress and strain relations takes the form of

$$\left[1 - (e_0 a)^2\nabla^2\right]\sigma_x = \frac{E(z)}{1 - \mu(z)^2}\left[\varepsilon_x + \mu(z)\varepsilon_\theta\right], \tag{12}$$

$$\left[1 - (e_0 a)^2\nabla^2\right]\sigma_\theta = \frac{E(z)}{1 - \mu(z)^2}\left[\varepsilon_\theta + \mu(z)\varepsilon_x\right], \tag{13}$$

$$\left[1 - (e_0 a)^2\nabla^2\right]\tau_{x\theta} = \frac{E(z)}{2[1 + \mu(z)]}\gamma_{x\theta}, \tag{14}$$

$$\left[1 - (e_0 a)^2\nabla^2\right]\tau_{\theta x} = \frac{E(z)}{2[1 + \mu(z)]}\gamma_{x\theta}, \tag{15}$$

where x and θ are longitudinal and angular circumferential coordinates, respectively; σ_x, σ_θ, $\tau_{x\theta}$ and $\tau_{\theta x}$ are normal and shear stresses; ε_x, ε_θ and $\gamma_{x\theta}$ are normal and shear strains; the Laplace operator is expressed as

$$\nabla^2 = \frac{\partial^2}{\partial x^2} + \frac{\partial^2}{r^2\partial\theta^2}, \tag{16}$$

where r is the middle-surface radius.

4 Wave propagation via nonlocal Flügge shell theory

Figure 1 shows an FGM circular cylindrical nanoshell with thickness h and middle-surface radius r. It is assumed that the cylindrical coordinate system (x, θ, z) is fixed at the midplane of the nanoshell.

Based on the Flügge shell theory [37], the displacements of an arbitrary point in the shell along the x-, θ-, z-axes, denoted by $u_x(x, \theta, z, t)$, $v_\theta(x, \theta, z, t)$ and $w_z(x, \theta, z, t)$, respectively, are

$$u_x(x, \theta, z, t) = u(x, \theta, t) - z\frac{\partial w(x, \theta, t)}{\partial x}, \tag{17}$$

$$v_\theta(x, \theta, z, t) = \frac{r + z}{r}v(x, \theta, t) - \frac{z}{r}\frac{\partial w(x, \theta, t)}{\partial\theta}, \tag{18}$$

$$w_z(x, \theta, z, t) = w(x, \theta, t), \tag{19}$$

where t is time; $u(x, \theta, t)$, $v(x, \theta, t)$ and $w(x, \theta, t)$ denote the displacements of a point at the midplane.

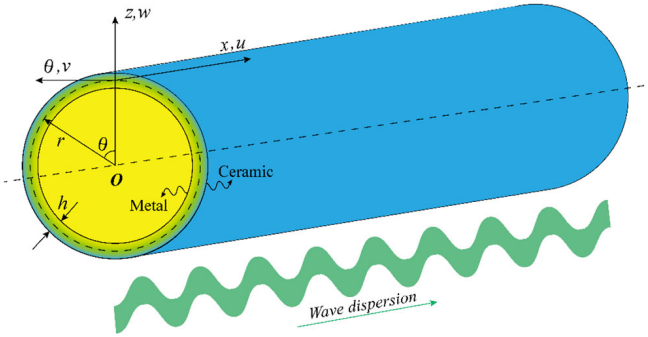

Fig. 1. Schematic diagram of FGM circular cylindrical nanoshell.

The relations between strains and displacements can be expressed as

$$\varepsilon_x = \frac{\partial u}{\partial x} - z\frac{\partial^2 w}{\partial x^2}, \tag{20}$$

$$\varepsilon_\theta = \frac{1}{r}\frac{\partial v}{\partial \theta} - \frac{z}{r(r+z)}\frac{\partial^2 w}{\partial \theta^2} + \frac{1}{r+z}w, \tag{21}$$

$$\gamma_{x\theta} = \frac{1}{r+z}\frac{\partial u}{\partial \theta} + \frac{r+z}{r}\frac{\partial v}{\partial x} - \left(\frac{z}{r} + \frac{z}{r+z}\right)\frac{\partial^2 w}{\partial x \partial \theta}. \tag{22}$$

The resultant forces and bending moments can be given as follows:

$$N_x = \int_{-h/2}^{h/2} \sigma_x \left(1 + \frac{z}{r}\right) \mathrm{d}z, \tag{23}$$

$$N_\theta = \int_{-h/2}^{h/2} \sigma_\theta \mathrm{d}z, \tag{24}$$

$$N_{x\theta} = \int_{-h/2}^{h/2} \tau_{x\theta} \left(1 + \frac{z}{r}\right) \mathrm{d}z, \tag{25}$$

$$N_{\theta x} = \int_{-h/2}^{h/2} \tau_{\theta x} \mathrm{d}z, \tag{26}$$

$$M_x = -\int_{-h/2}^{h/2} \sigma_x \left(1 + \frac{z}{r}\right) z \, \mathrm{d}z, \tag{27}$$

$$M_\theta = -\int_{-h/2}^{h/2} \sigma_\theta z \, \mathrm{d}z, \tag{28}$$

$$M_{x\theta} = -\int_{-h/2}^{h/2} \tau_{x\theta} \left(1 + \frac{z}{r}\right) z \, \mathrm{d}z, \tag{29}$$

$$M_{\theta x} = -\int_{-h/2}^{h/2} \tau_{\theta x} z \, \mathrm{d}z. \tag{30}$$

From eqs. (12)–(15) and (20)–(30), we obtain

$$\left[1 - (e_0 a)^2 \nabla^2\right] N_x = B_{11}\frac{\partial u}{\partial x} - B_{12}\frac{\partial^2 w}{\partial x^2} + B_{13}\frac{1}{r}\frac{\partial v}{\partial \theta} - B_{14}\frac{1}{r}\frac{\partial^2 w}{\partial \theta^2} + B_{15}w, \tag{31}$$

$$\left[1 - (e_0 a)^2 \nabla^2\right] N_\theta = A_{21}\frac{1}{r}\frac{\partial v}{\partial \theta} - A_{22}\frac{1}{r}\frac{\partial^2 w}{\partial \theta^2} + A_{23}w + A_{24}\frac{\partial u}{\partial x} - A_{25}\frac{\partial^2 w}{\partial x^2}, \tag{32}$$

$$\left[1-(e_0a)^2\nabla^2\right]N_{x\theta}=B_{31}\frac{\partial u}{\partial\theta}+B_{32}\frac{1}{r}\left(\frac{\partial v}{\partial x}-\frac{\partial^2 w}{\partial x\partial\theta}\right)+B_{33}\frac{\partial v}{\partial x}-B_{34}\frac{\partial^2 w}{\partial x\partial\theta}, \tag{33}$$

$$\left[1-(e_0a)^2\nabla^2\right]N_{\theta x}=A_{31}\frac{\partial u}{\partial\theta}+A_{32}\frac{1}{r}\left(\frac{\partial v}{\partial x}-\frac{\partial^2 w}{\partial x\partial\theta}\right)+A_{33}\frac{\partial v}{\partial x}-A_{34}\frac{\partial^2 w}{\partial x\partial\theta}, \tag{34}$$

$$\left[1-(e_0a)^2\nabla^2\right]M_x=-D_{11}\frac{\partial u}{\partial x}+D_{12}\frac{\partial^2 w}{\partial x^2}-D_{13}\frac{1}{r}\frac{\partial v}{\partial\theta}+D_{14}\frac{1}{r}\frac{\partial^2 w}{\partial\theta^2}-D_{15}w, \tag{35}$$

$$\left[1-(e_0a)^2\nabla^2\right]M_\theta=-C_{21}\frac{1}{r}\frac{\partial v}{\partial\theta}+C_{22}\frac{1}{r}\frac{\partial^2 w}{\partial\theta^2}-C_{23}w-C_{24}\frac{\partial u}{\partial x}+C_{25}\frac{\partial^2 w}{\partial x^2}, \tag{36}$$

$$\left[1-(e_0a)^2\nabla^2\right]M_{x\theta}=-D_{31}\frac{\partial u}{\partial\theta}-D_{32}\frac{1}{r}\left(\frac{\partial v}{\partial x}-\frac{\partial^2 w}{\partial x\partial\theta}\right)-D_{33}\frac{\partial v}{\partial x}+D_{34}\frac{\partial^2 w}{\partial x\partial\theta}, \tag{37}$$

$$\left[1-(e_0a)^2\nabla^2\right]M_{\theta x}=-C_{31}\frac{\partial u}{\partial\theta}-C_{32}\frac{1}{r}\left(\frac{\partial v}{\partial x}-\frac{\partial^2 w}{\partial x\partial\theta}\right)-C_{33}\frac{\partial v}{\partial x}+C_{34}\frac{\partial^2 w}{\partial x\partial\theta}, \tag{38}$$

where the parameters A_{ij}, B_{ij}, C_{ij} and D_{ij} $(i,\,j=1,2,\ldots,5)$ are given in appendix A, from which one can obtain the analytical computation results of the integrals.

The equilibriums of resultant forces and bending moments of the FGM cylindrical nanoshell can be expressed as [37]

$$r\frac{\partial N_x}{\partial x}+\frac{\partial N_{\theta x}}{\partial\theta}+Ir\frac{\partial^2 u}{\partial t^2}=0, \tag{39}$$

$$r\frac{\partial N_\theta}{\partial\theta}+r^2\frac{\partial N_{x\theta}}{\partial x}-\frac{\partial M_\theta}{\partial\theta}-r\frac{\partial M_{x\theta}}{\partial x}+Ir^2\frac{\partial^2 v}{\partial t^2}=0, \tag{40}$$

$$\frac{\partial^2 M_\theta}{\partial\theta^2}+r\frac{\partial^2 M_{x\theta}}{\partial x\partial\theta}+r\frac{\partial^2 M_{\theta x}}{\partial x\partial\theta}+r^2\frac{\partial^2 M_x}{\partial x^2}+rN_\theta-Ir^2\frac{\partial^2 w}{\partial t^2}=0, \tag{41}$$

where the coefficient I takes the form of

$$I=\int_{-h/2}^{h/2}\rho(z)\mathrm{d}z. \tag{42}$$

By substituting eqs. (31)–(38) into eqs. (39)–(41), the governing equations can be obtained as

$$\begin{aligned}&B_{11}r^2\frac{\partial^2 u}{\partial x^2}+A_{31}r\frac{\partial^2 u}{\partial\theta^2}+\left[A_{32}+(A_{33}+B_{13})\,r\right]\frac{\partial^2 v}{\partial x\partial\theta}+B_{15}r^2\frac{\partial w}{\partial x}-B_{12}r^2\frac{\partial^3 w}{\partial x^3}\\&-\left[A_{32}+(A_{34}+B_{14})r\right]\frac{\partial^3 w}{\partial x\partial\theta^2}+Ir^2\left[1-(e_0a)^2\nabla^2\right]\frac{\partial^2 u}{\partial t^2}=0,\end{aligned} \tag{43}$$

$$\begin{aligned}&\left[C_{24}r+(D_{31}+A_{24})r^2+B_{31}r^3\right]\frac{\partial^2 u}{\partial x\partial\theta}+\left[D_{32}r+(B_{32}+D_{33})\,r^2+B_{33}r^3\right]\frac{\partial^2 v}{\partial x^2}\\&+(C_{21}+A_{21}r)\frac{\partial^2 v}{\partial\theta^2}+\left(C_{23}r+A_{23}r^2\right)\frac{\partial w}{\partial\theta}-(C_{22}+A_{22}r)\frac{\partial^3 w}{\partial\theta^3}\\&-\left[(C_{25}+D_{32})r+(A_{25}+B_{32}+D_{34})r^2+B_{34}r^3\right]\frac{\partial^3 w}{\partial x^2\partial\theta}+Ir^3\left[1-(e_0a)^2\nabla^2\right]\frac{\partial^2 v}{\partial t^2}=0,\end{aligned} \tag{44}$$

$$\begin{aligned}&D_{11}r^3\frac{\partial^3 u}{\partial x^3}-A_{24}r^2\frac{\partial u}{\partial x}+\left[C_{24}r+(C_{31}+D_{31})r^2\right]\frac{\partial^3 u}{\partial x\partial\theta^2}\\&+\left[(C_{32}+D_{32})r+(C_{33}+D_{13}+D_{33})r^2\right]\frac{\partial^3 v}{\partial x^2\partial\theta}+C_{21}\frac{\partial^3 v}{\partial\theta^3}-A_{21}r\frac{\partial v}{\partial\theta}-D_{12}r^3\frac{\partial^4 w}{\partial x^4}\\&+(A_{25}r^2+D_{15}r^3)\frac{\partial^2 w}{\partial x^2}-\left[(C_{25}+C_{32}+D_{32})r+(C_{34}+D_{14}+D_{34})r^2\right]\frac{\partial^4 w}{\partial x^2\partial\theta^2}\\&+(A_{22}+C_{23})r\frac{\partial^2 w}{\partial\theta^2}-C_{22}\frac{\partial^4 w}{\partial\theta^4}-A_{23}r^2w+Ir^3\left[1-(e_0a)^2\nabla^2\right]\frac{\partial^2 w}{\partial t^2}=0.\end{aligned} \tag{45}$$

The wave propagation solution of eqs. (43)–(45) can be written as

$$u(x,\theta,t) = Ue^{\mathrm{i}(kx+n\theta-\omega t)}, \tag{46}$$

$$v(x,\theta,t) = Ve^{\mathrm{i}(kx+n\theta-\omega t)}, \tag{47}$$

$$w(x,\theta,t) = We^{\mathrm{i}(kx+n\theta-\omega t)}, \tag{48}$$

where U, V and W are the amplitudes of wave motion; ω is the frequency of wave motion; k and n are the wave number in the longitudinal and circumferential directions, respectively.

The relation between the phase velocity v and wave frequency ω can be expressed as follows [31]:

$$v = \omega/k. \tag{49}$$

Substituting eqs. (46)–(48) into eqs. (43)–(45) yields a generalized eigenvalue problem

$$\left(L_{3\times3} - \omega^2 H_{3\times3}\right)\begin{Bmatrix} U \\ V \\ W \end{Bmatrix} = \{0\}, \tag{50}$$

where the elements L_{ij} and H_{ij} (i, $j = 1, 2, 3$) in the matrix $L_{3\times3}$ and $H_{3\times3}$ are given in appendix B. The dispersion relation derived from eq. (50) takes the form

$$\mathrm{Det}\left[L_{3\times3} - \omega^2 H_{3\times3}\right] = 0. \tag{51}$$

According to eq. (51), the analytical solutions of wave frequency are obtained by using the "Mathematica" software. Since the analytical formulas of wave frequency are too long, they are not written here. If all parameters are substituted in the analytical formulas, the frequency values can be obtained by using the "Mathematica" software.

Three cut-off frequencies can be obtained by setting the longitudinal wave number $k = 0$:

$$\omega_{c1}^2 = \frac{A_{31}n^2 r}{I[(e_0 a)^2 n^2 + r^2]}, \tag{52}$$

$$\omega_{c2}^2 = \frac{\chi_2}{I[(e_0 a)^2 n^2 + r^2]}, \tag{53}$$

$$\omega_{c3}^2 = \frac{\chi_3}{I[(e_0 a)^2 n^2 + r^2]}, \tag{54}$$

where

$$\chi_2 = \frac{1}{2r}(\xi - \sqrt{\zeta}), \tag{55}$$

$$\chi_3 = \frac{1}{2r}(\xi + \sqrt{\zeta}) \tag{56}$$

and

$$\xi = A_{21}n^2 r + A_{22}n^2 r + A_{23}r^2 + C_{21}n^2 + C_{22}n^4 + C_{23}n^2 r \tag{57}$$

$$\begin{aligned}\zeta = {} & A_{21}^2 n^4 r^2 + A_{22}^2 n^4 r^2 + A_{23}^2 r^4 - 2A_{23}C_{21}n^2 r^2 + 4A_{23}C_{21}n^4 r^2 + C_{21}^2 n^4 \\ & + 2A_{23}C_{22}n^4 r^2 + 2C_{21}C_{22}n^6 + C_{22}^2 n^8 + 2C_{23}\left(A_{23}r^2 + C_{21}n^2 + C_{22}n^4\right)n^2 r \\ & + C_{23}^2 n^4 r^2 + 2A_{22}n^2 r\left[-C_{21}n^2 + n^4(2C_{21} + C_{22}) + r(A_{23}r + C_{23}n^2)\right] \\ & + 2A_{21}n^2 r\left[A_{22}n^2 r + A_{23}r^2 + 2C_{23}r + (C_{21} + 2C_{22} - C_{22}n^2 - C_{23}r)n^2\right].\end{aligned} \tag{58}$$

5 Results and discussion

In order to examine the validity of the present analysis, we first make a comparison study for a homogeneous cylindrical nanoshell. The mass density, Poisson's ratio, thickness and radius of the cylindrical nanoshells are $\rho = 2.27\,\mathrm{g/cm^3}$, $\mu = 0.2$, $h = 0.34\,\mathrm{nm}$ and $r = 5\,\mathrm{nm}$, respectively. The in-plane stiffness is $Eh = 360\,\mathrm{J/m^2}$ and the bending rigidity is $D = 2\,\mathrm{eV}$. In fig. 2, it can be seen that very good agreement between the present results and those in the literature has been achieved, bespeaking the validity of the present analysis.

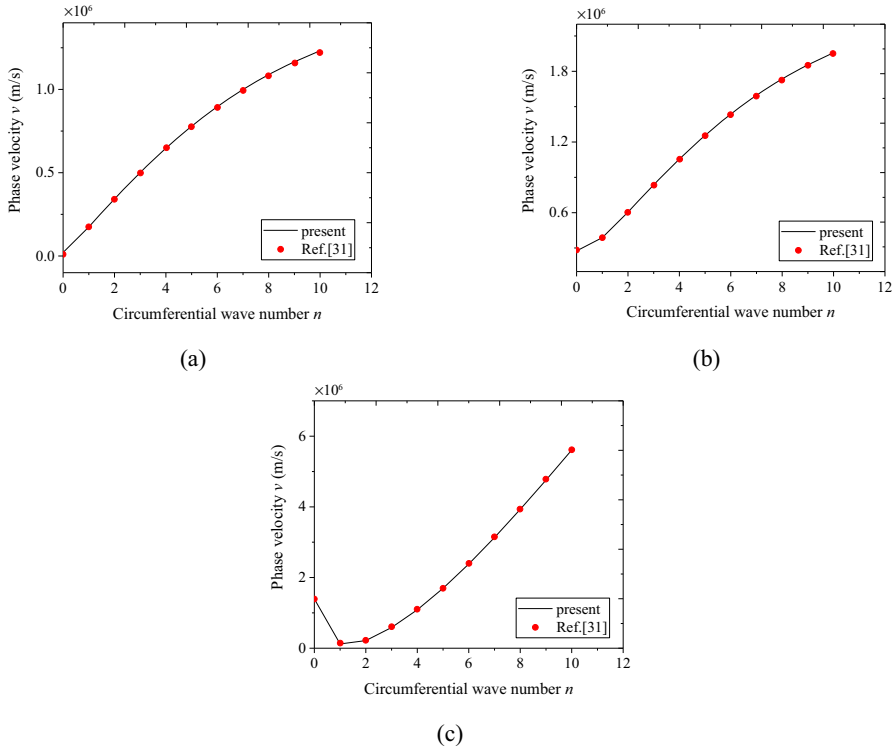

Fig. 2. Comparisons of wave characteristics in a homogenous cylindrical nanoshell ($k = 8 \times 10^6\,\mathrm{m}^{-1}$, $e_0a = 1\,\mathrm{nm}$): (a) the first mode; (b) the second mode; and (c) the third mode.

Table 1. Properties of materials [38].

	Nickel			Al_2O_3		
	E (Pa)	ρ (kg/m^3)	μ	E (Pa)	ρ (kg/m^3)	μ
P_{-1}	0	0	0	0	0	0
P_0	205.098×10^9	8900	0.31	349.55×10^9	3950	0.26
P_1	-2.794×10^{-4}	0	0	-3.853×10^{-4}	0	0
P_2	-3.998×10^{-9}	0	0	-4.027×10^{-7}	0	0
P_3	0	0	0	-1.673×10^{-10}	0	0
$T = 300\,\mathrm{K}$	187.833×10^9	8900	0.31	294.898×10^9	3950	0.26

In what follows, wave propagation in the FGM circular cylindrical nanoshell shown in fig. 1 will be dealt with. The FGM nanoshell is composed of metal (nickel) and ceramic (Al_2O_3); and the inner and outer surfaces are full metal and full ceramic, respectively. The material properties are tabulated in table 1. If not specified, the room temperature ($T = 300\,\mathrm{K}$) is considered and the thickness and middle-surface radius of the cylindrical nanoshell are fixed as $h = 1\,\mathrm{nm}$ and $r = 50\,\mathrm{nm}$, respectively.

The cut-off frequencies *versus* circumferential wave number n are tabulated in table 2 for FGM nanoshells with different power-law exponents, namely, $p = 0, 1, 5$, where $e_0a = 1\,\mathrm{nm}$. As can be observed, only one cut-off frequency exists when $n = 0$ (axisymmetric motion). Moreover, when $n = 1$, two cut-off frequencies exist. Three cut-off frequencies exist only when $n \geq 2$. It is noted that the cut-off frequencies increase with increasing circumferential wave number n. In addition, an increase in power-law exponent leads to a decrease in cut-off frequencies of the FGM nanoshells.

In figs. 3 and 4, the curves of phase velocity *versus* longitudinal wave number k for the first three modes are given for $n = 0$ (axisymmetric motion) and $n = 1$ (asymmetric motion), respectively, where $e_0a = 1\,\mathrm{nm}$. The comparison of figs. 3(a) and 4(a) shows that at small longitudinal wave number, the phase velocity for the first mode exhibits an increasing-trend variation at $n = 1$, but the phase velocity is constant at $n = 0$. In figs. 3(c) and 4(c), at small longitudinal wave number, the phase velocity for the third mode shows a decreasing-trend variation when $n = 1$; and the phase velocity remains constant when $n = 0$. It is also noted that the circumferential wave number n has invisible effect on the phase velocity for the second mode, as can be seen in figs. 3(b) and 4(b). The effect of the power-law exponent on wave propagation characteristics in the FGM cylindrical nanoshell is also highlighted in these figures. It is found that the increase of power-law exponent results in the decrease of the phase velocity.

Table 2. Cut-off frequencies (GHz) of FGM nanoshell ($e_0a = 1\,\text{nm}$).

n	$p=0$			$p=1$			$p=5$		
0	179			127.8			105.8		
1	253		108.8	180.8		76.5	149.7		62.6
2	399.9	2.8	217.5	285.8	2	152.9	236.6	1.7	125.1
3	564.9	7.8	326	403.9	5.5	229.1	334.3	4.7	187.4
4	735.5	15	434.1	525.9	10.6	305	435.3	9.1	249.5
5	908	24.2	541.6	649.2	17.1	380.6	537.4	14.6	311.4
6	1080.9	35.4	648.5	772.8	25.1	455.7	639.7	21.4	372.8
7	1253.3	48.6	754.7	896.1	34.4	530.3	741.7	29.4	433.8
8	1424.8	63.8	860	1018.7	45.2	604.3	843.2	38.6	494.4
9	1595	80.9	964.3	1140.5	57.2	677.6	944	48.9	554.3
10	1763.7	99.8	1067.5	1261.1	70.7	750.1	1043.8	60.3	613.7

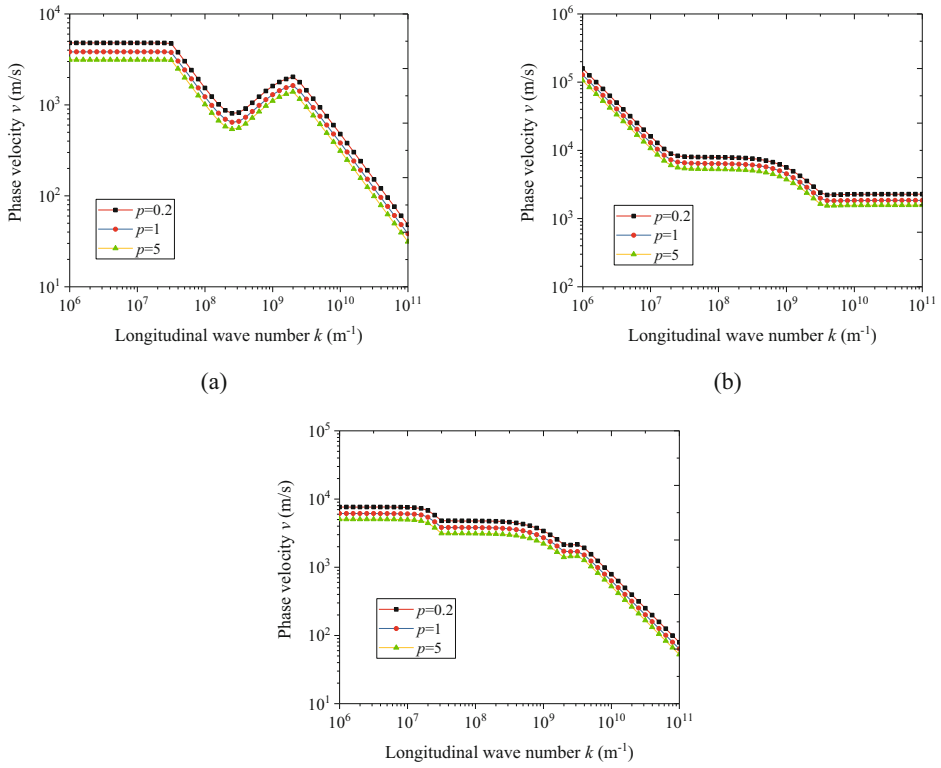

Fig. 3. Phase velocity *versus* longitudinal wave number k of FGM nanoshell ($n = 0$): (a) the first mode; (b) the second mode; and (c) the third mode.

The dispersion relation between the phase velocity and circumferential wave number n is depicted in fig. 5 at relative small longitudinal wave number $k = 10^7\,\text{m}^{-1}$, where $e_0a = 1\,\text{nm}$. It can be seen that phase velocities of the first and second modes increase with the circumferential wave number. As for the third mode, phase velocity decreases initially and then increases with the circumferential wave number. It is found that the lowest phase velocity occurs at $n = 3$.

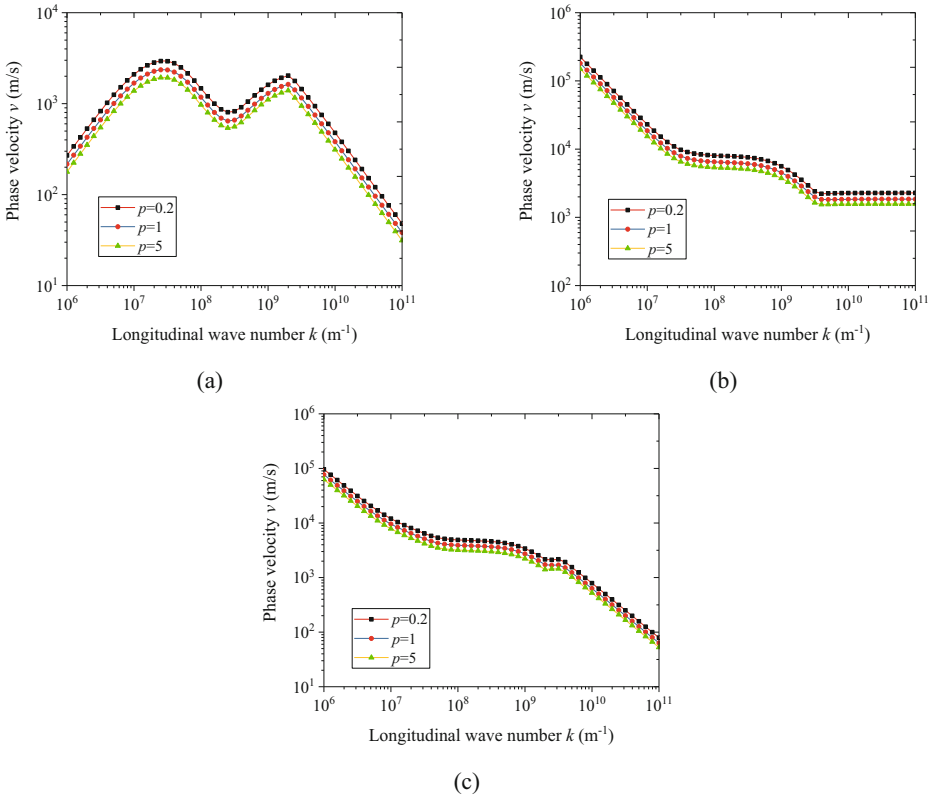

Fig. 4. Phase velocity *versus* longitudinal wave number k of FGM nanoshell ($n = 1$): (a) the first mode; (b) the second mode; and (c) the third mode.

Figure 6 demonstrates the curves of phase velocity *versus* circumferential wave number n at relative large longitudinal wave number $k = 10^9\,\mathrm{m}^{-1}$, where the other parameters used are the same as fig. 5. It can be seen that the phase velocities vary slightly with the circumferential wave number. This indicates that the circumferential wave number has insignificant effect on the phase velocity of FGM nanoshells when the longitudinal wave number is large, which is different from the case of small longitudinal wave number shown in fig. 5.

Figures 7 and 8 depict the effect of nonlocal parameter e_0a on the dispersion relations of FGM cylindrical nanoshell for $n = 0$ (axisymmetric motion) and $n = 1$ (asymmetric motion), respectively, where $p = 1$. It can be seen that when longitudinal wave number $k < 10^8\,\mathrm{m}^{-1}$, invisible difference of the phase velocities between the *local* and *nonlocal* shell models is found, showing the applicability of the local ($e_0a = 0$) Flügge shell theory when the longitudinal wave number is small. However, when the longitudinal wave number $k > 10^8\,\mathrm{m}^{-1}$, the phase velocity via the nonlocal shell model is obviously different from that via the local model, indicating that the *nonlocal* shell model must be adopted for large longitudinal wave number. Moreover, the phase velocities for the three modes decrease with the small scale parameter. It is also noted from figs. 7(a) and (c) that, when the longitudinal wave number is small, the phase velocities for the first and third modes remain constant at $n = 0$. When $n = 1$, however, the phase velocities for the first and third modes exhibit nonuniform variation, as shown in figs. 8(a) and (c).

In fig. 9, the nonlocal parameter effect on the dispersion relations between the phase velocity and circumferential wave number n is shown, where $p = 1$, $k = 10^7\,\mathrm{m}^{-1}$. Invisible difference of the phase velocities between the *local* and *nonlocal* shell models is found when circumferential wave number $n < 4$, indicating the local Flügge shell theory is acceptable for small circumferential wave number. When $n > 4$, however, an increase in the small scale parameter leads to the decreasing phase velocity. It means that the local Flügge shell theory is not applicable to provide accurate dispersion relations when the circumferential wave number n is large. In this case, the nonlocal Flügge shell theory should be employed.

In fig. 10, the phase velocity ratio *versus* small scale parameter e_0a is shown for the first mode at three different power-law exponents, namely, $p = 0.2, 1$ and 5. The phase velocity ratio is defined by the phase velocity obtained via the nonlocal Flügge shell model to that via the local model. It is clear that the phase velocity ratio is unit when $e_0a = 0$. In addition, an increase in the small scale parameter results in the decrease in the phase velocity ratio. It is also found that the phase velocity ratio decreases with increasing longitudinal wave number.

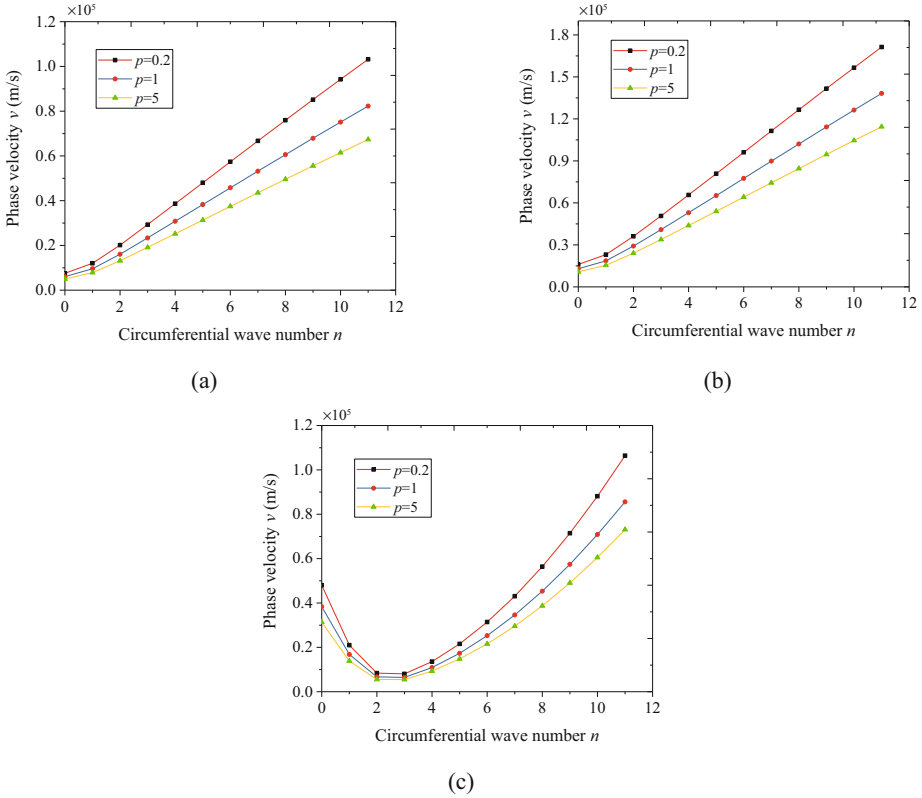

Fig. 5. Phase velocity *versus* circumferential wave number n of FGM nanoshell ($k = 10^7\,\mathrm{m}^{-1}$): (a) the first mode; (b) the second mode; and (c) the third mode.

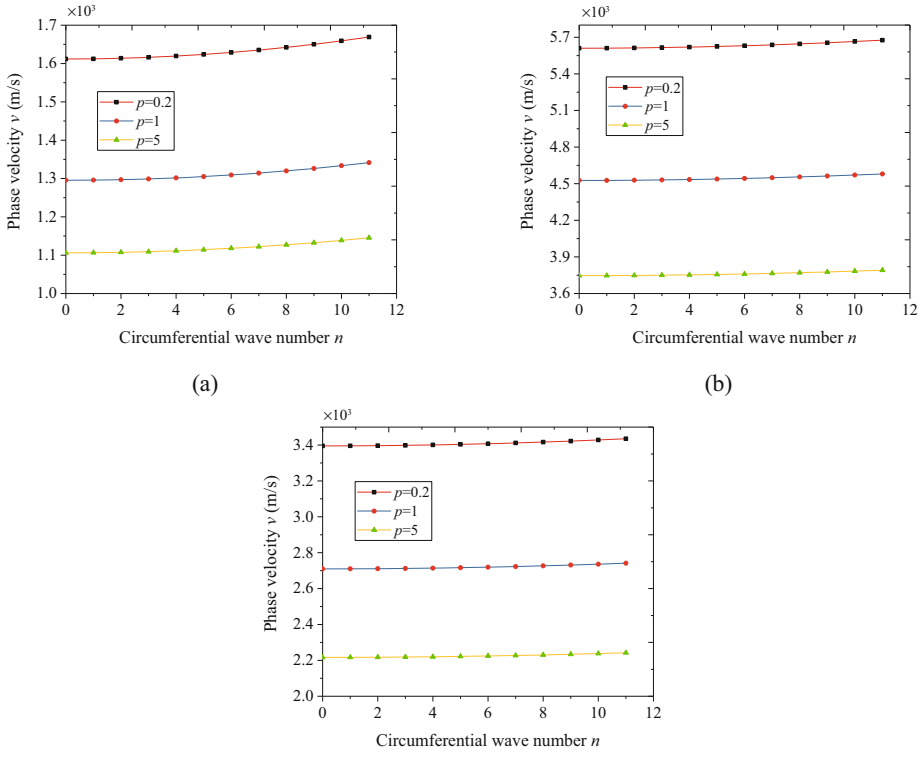

Fig. 6. Phase velocity *versus* circumferential wave number n of FGM nanoshell ($k = 10^9\,\mathrm{m}^{-1}$): (a) the first mode; (b) the second mode; and (c) the third mode.

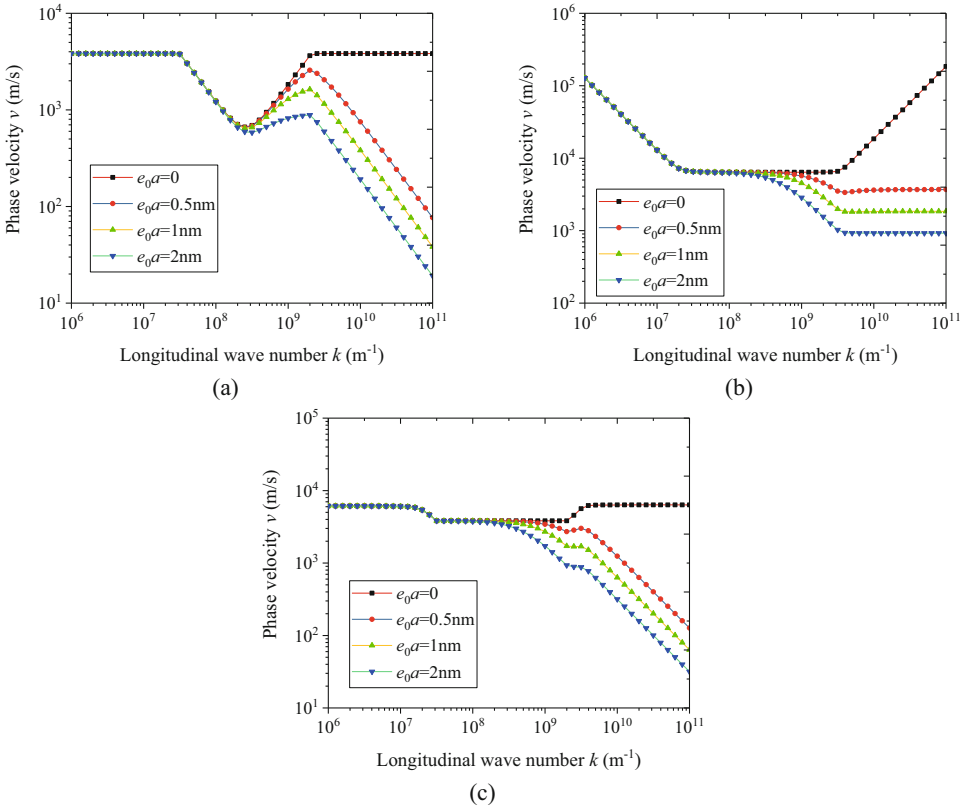

Fig. 7. Phase velocity *versus* longitudinal wave number k of FGM nanoshell ($n = 0$): (a) the first mode; (b) the second mode; and (c) the third mode.

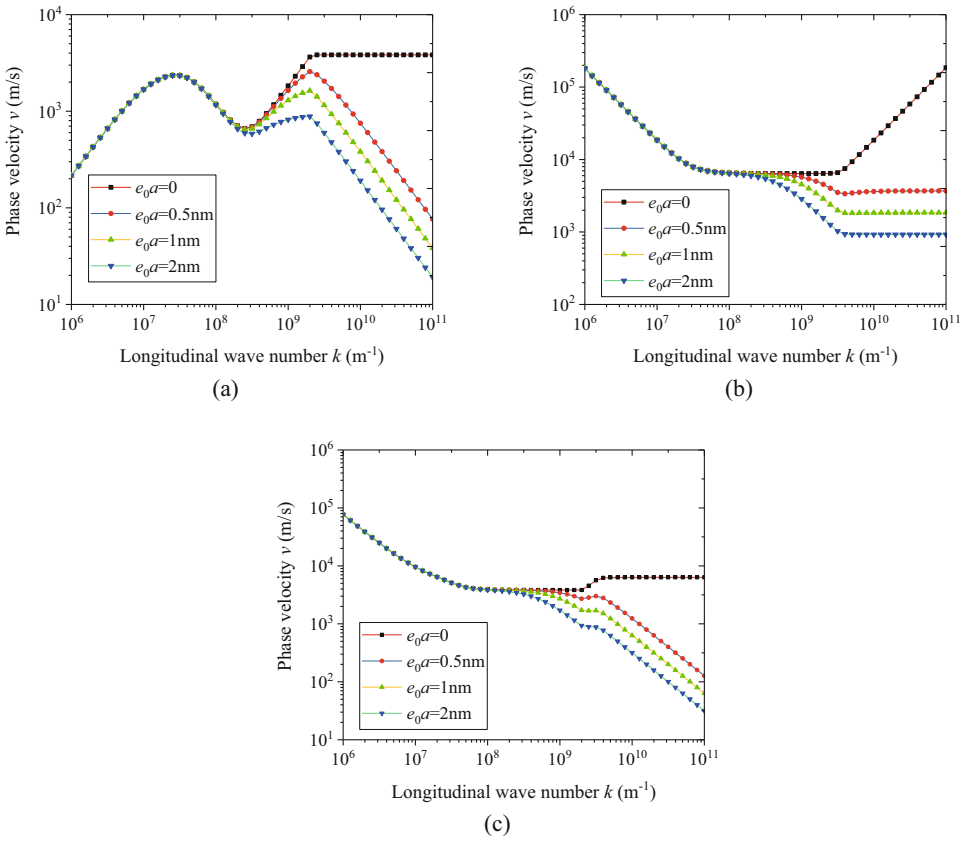

Fig. 8. Phase velocity *versus* longitudinal wave number k of FGM nanoshell ($n = 1$): (a) the first mode; (b) the second mode; and (c) the third mode.

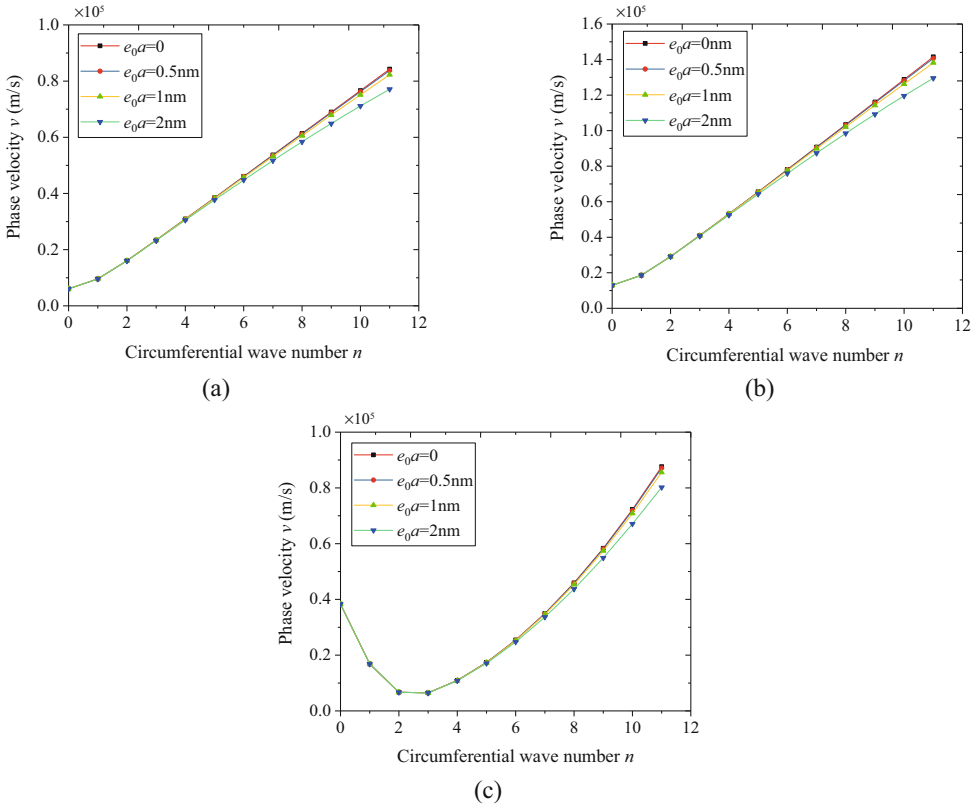

Fig. 9. Phase velocity *versus* circumferential wave number n of FGM nanoshell: (a) the first mode; (b) the second mode; and (c) the third mode.

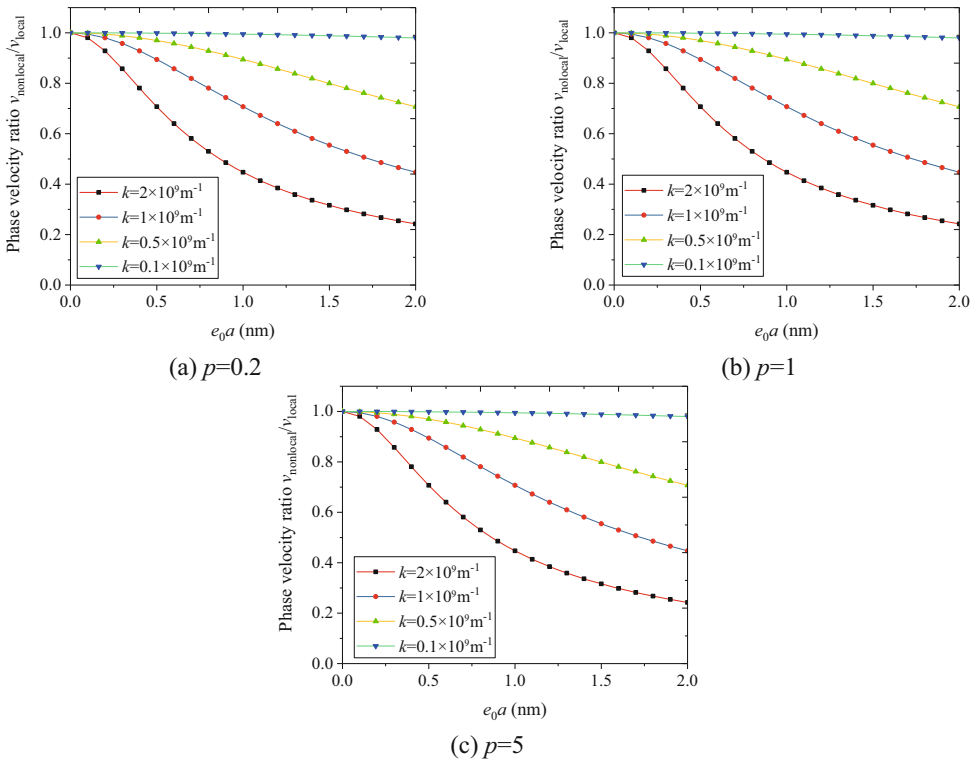

Fig. 10. The phase velocity ratio ($v_{\mathrm{nonlocal}}/v_{\mathrm{local}}$) for the first mode ($n = 1$).

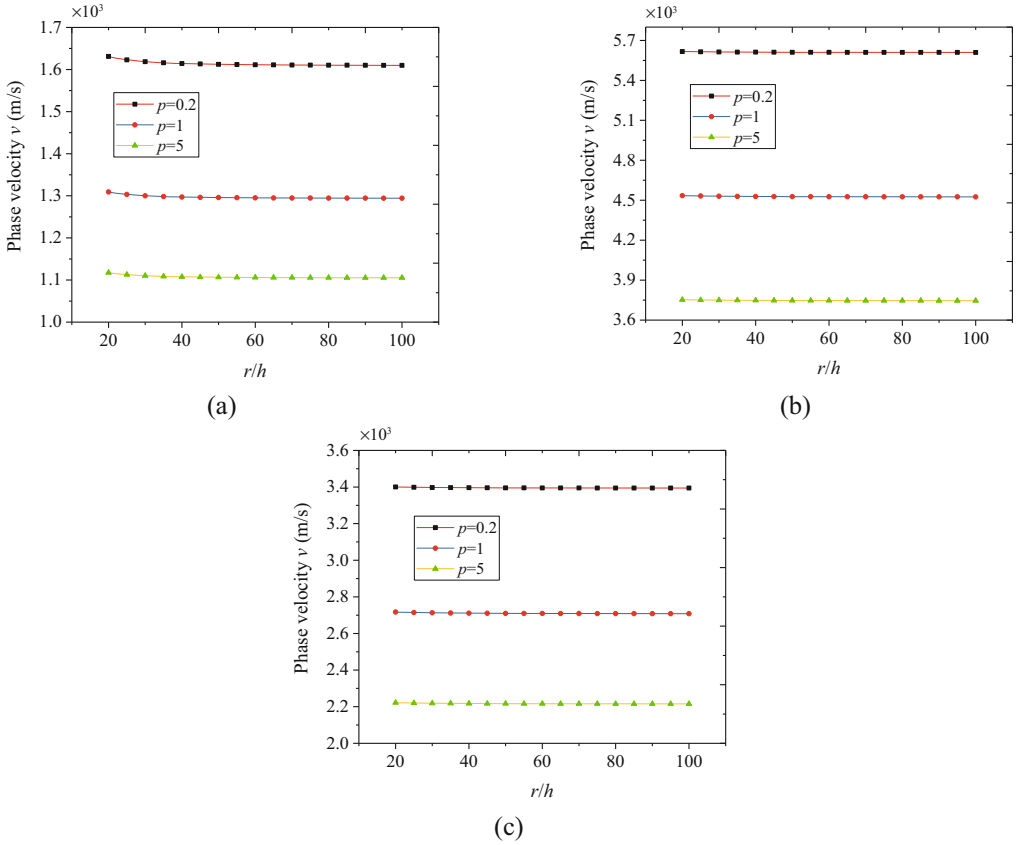

Fig. 11. Phase velocity *versus* radius-to-thickness ratio via nonlocal Flügge shell theory: (a) the first mode; (b) the second mode; and (c) the third mode.

In fig. 11, the phase velocity *versus* radius-to-thickness ratio for the first three modes is given via the nonlocal Flügge shell theory, where $e_0a = 1\,\mathrm{nm}$, $k = 10^9\,\mathrm{m}^{-1}$ and $n = 1$. As can be observed, the phase velocity is insensitive to the radius-to-thickness ratio of the FGM nanoshells. This is a distinct and interesting result since the radius-to-thickness ratio has obvious effect on the vibration and buckling behavior of FGM nanoshells [39,40].

6 Concluding remarks

In this paper, wave propagation characteristics of FGM circular cylindrical nanoshells are investigated based on the nonlocal elasticity theory and the Flügge shells theory. Detailed wave dispersion results with respect to the longitudinal and circumferential wave numbers, the power-law exponent, the small scale parameter and the radius-to-thickness ratio are explicitly analyzed. It is shown that the larger power-law exponent leads to the smaller phase velocity in the FGM nanoshells. When the longitudinal or circumferential wave number is small, the small scale effect is negligible and the *local* shell theory can be applied, whereas, at large longitudinal or circumferential wave number, the nonlocal effect is significant and the *nonlocal* Flügge shell theory should be employed to provide more accurate wave solutions. The results also show that the variation of the radius-to-thickness ratio has negligible effect on the wave propagation of the FGM nanoshells.

This research was supported by the National Natural Science Foundation of China (Grant no. 11672071) and the Fundamental Research Funds for the Central Universities (Grant no. N170504023).

Appendix A.

$$A_{21}=\int_{-h/2}^{h/2}\frac{E(z)}{1-\mu(z)^2}\mathrm{d}z,\quad A_{22}=\int_{-h/2}^{h/2}\frac{E(z)}{1-\mu(z)^2}\left(\frac{z}{r+z}\right)\mathrm{d}z,\quad A_{23}=\int_{-h/2}^{h/2}\frac{E(z)}{1-\mu(z)^2}\left(\frac{1}{r+z}\right)\mathrm{d}z,$$

$$A_{24}=\int_{-h/2}^{h/2}\frac{E(z)\mu(z)}{1-\mu(z)^2}\mathrm{d}z,\quad A_{25}=\int_{-h/2}^{h/2}\frac{E(z)\mu(z)}{1-\mu(z)^2}z\,\mathrm{d}z,\quad A_{31}=\int_{-h/2}^{h/2}\frac{E(z)}{2[1+\mu(z)]}\left(\frac{1}{r+z}\right)\mathrm{d}z,$$

$$A_{32}=\int_{-h/2}^{h/2}\frac{E(z)}{2\,[1+\mu(z)]}z\,\mathrm{d}z,\quad A_{33}=\int_{-h/2}^{h/2}\frac{E(z)}{2[1+\mu(z)]}\mathrm{d}z,\quad A_{34}=\int_{-h/2}^{h/2}\frac{E(z)}{2[1+\mu(z)]}\left(\frac{z}{r+z}\right)\mathrm{d}z,$$

$$B_{11}=\int_{-h/2}^{h/2}\frac{E(z)}{1-\mu(z)^2}\left(\frac{r+z}{r}\right)\mathrm{d}z,\quad B_{12}=\int_{-h/2}^{h/2}\frac{E(z)}{1-\mu(z)^2}\left(\frac{r+z}{r}\right)z\,\mathrm{d}z,\quad B_{13}=\int_{-h/2}^{h/2}\frac{E(z)\mu(z)}{1-\mu(z)^2}\left(\frac{r+z}{r}\right)\mathrm{d}z,$$

$$B_{14}=\int_{-h/2}^{h/2}\frac{E(z)\mu(z)}{1-\mu(z)^2}\left(\frac{z}{r}\right)\mathrm{d}z,\quad B_{15}=\int_{-h/2}^{h/2}\frac{E(z)\mu(z)}{1-\mu(z)^2}\left(\frac{1}{r}\right)\mathrm{d}z,\quad B_{31}=\int_{-h/2}^{h/2}\frac{E(z)}{2[1+\mu(z)]}\left(\frac{1}{r}\right)\mathrm{d}z,$$

$$B_{32}=\int_{-h/2}^{h/2}\frac{E(z)}{2[1+\mu(z)]}\left(\frac{r+z}{r}\right)z\,\mathrm{d}z,\quad B_{33}=\int_{-h/2}^{h/2}\frac{E(z)}{2[1+\mu(z)]}\left(\frac{r+z}{r}\right)\mathrm{d}z,\quad B_{34}=\int_{-h/2}^{h/2}\frac{E(z)}{2[1+\mu(z)]}\left(\frac{z}{r}\right)\mathrm{d}z,$$

$$C_{21}=\int_{-h/2}^{h/2}\frac{E(z)}{1-\mu(z)^2}z\,\mathrm{d}z,\quad C_{22}=\int_{-h/2}^{h/2}\frac{E(z)}{1-\mu(z)^2}\left(\frac{z}{r+z}\right)z\,\mathrm{d}z,$$

$$C_{23}=A_{22},\quad C_{24}=A_{25},\quad C_{25}=\int_{-h/2}^{h/2}\frac{E(z)\mu(z)}{1-\mu(z)^2}z^2\mathrm{d}z,$$

$$C_{31}=A_{34},\quad C_{32}=\int_{-h/2}^{h/2}\frac{E(z)}{2[1+\mu(z)]}z^2\mathrm{d}z,\quad C_{33}=A_{32},$$

$$C_{34}=\int_{-h/2}^{h/2}\frac{E(z)}{2[1+\mu(z)]}\left(\frac{z}{r+z}\right)z\,\mathrm{d}z,\quad D_{11}=B_{12},$$

$$D_{12}=\int_{-h/2}^{h/2}\frac{E(z)}{1-\mu(z)^2}\left(\frac{r+z}{r}\right)z^2\mathrm{d}z,\quad D_{13}=\int_{-h/2}^{h/2}\frac{E(z)\mu(z)}{1-\mu(z)^2}\left(\frac{r+z}{r}\right)z\,\mathrm{d}z,$$

$$D_{14}=\int_{-h/2}^{h/2}\frac{E(z)\mu(z)}{1-\mu(z)^2}\left(\frac{z}{r}\right)z\,\mathrm{d}z,\quad D_{15}=B_{14},\quad D_{31}=B_{34},$$

$$D_{32}=\int_{-h/2}^{h/2}\frac{E(z)}{2[1+\mu(z)]}\left(\frac{r+z}{r}\right)z^2\mathrm{d}z,\quad D_{33}=B_{32},\quad D_{34}=\int_{-h/2}^{h/2}\frac{E(z)}{2[1+\mu(z)]}\left(\frac{z}{r}\right)z\,\mathrm{d}z.$$

Appendix B.

$$L_{11}=A_{31}n^2r+B_{11}k^2r^2,$$

$$L_{12}=[A_{32}+(A_{33}+B_{13})r]kn,$$

$$L_{13}=-\mathrm{i}k\left[A_{32}n^2+(A_{34}+B_{14})n^2r+\left(B_{15}+B_{12}k^2\right)r^2\right],$$

$$L_{21}=\mathrm{i}knr\left(A_{24}r+B_{31}r^2+C_{24}+D_{31}r\right),$$

$$L_{22}=\mathrm{i}\left(A_{21}n^2r+B_{32}k^2r^2+B_{33}k^2r^3+C_{21}n^2+D_{32}k^2r+D_{33}k^2r^2\right),$$

$$L_{23}=A_{22}n^3r+A_{23}nr^2+A_{25}k^2nr^2+B_{32}k^2nr^2+B_{34}k^2nr^3+C_{22}n^3+C_{23}nr+C_{25}k^2nr+D_{32}k^2nr+D_{34}k^2nr^2,$$

$$L_{31}=\mathrm{i}kr\left(A_{24}r+C_{24}n^2+C_{31}n^2r+D_{11}k^2r^2+D_{31}n^2r\right),$$

$$L_{32}=\mathrm{i}n\left(A_{21}r+C_{21}n^2+C_{32}k^2r+C_{33}k^2r^2+D_{13}k^2r^2+D_{32}k^2r+D_{33}k^2r^2\right),$$

$$\begin{aligned}L_{33}=&A_{22}n^2r+A_{23}r^2+A_{25}k^2r^2+C_{22}n^4+C_{23}n^2r+C_{25}k^2n^2r+C_{32}k^2n^2r+C_{34}k^2n^2r^2\\&+D_{12}k^4r^3+D_{14}k^2n^2r^2+D_{15}k^2r^3+D_{32}k^2n^2r+D_{34}k^2n^2r^2,\end{aligned}$$

$$H_{11}=I\left[r^2+(e_0a)^2\left(n^2+k^2r^2\right)\right],\quad H_{12}=H_{13}=0,$$

$$H_{21}=H_{23}=0,\quad H_{22}=\mathrm{i}Ir\left[r^2+(e_0a)^2\left(n^2+k^2r^2\right)\right],$$

$$H_{31}=H_{32}=0,\quad H_{33}=Ir\left[r^2+(e_0a)^2\left(n^2+k^2r^2\right)\right].$$

References

1. M. Koizumi, Composites Part B **28**, 1 (1997).
2. G.L. She, K.M. Yan, Y.L. Zhang, H.B. Liu, Y.R. Ren, Eur. Phys. J. Plus **133**, 368 (2018).
3. Y.Q. Wang, J.W. Zu, Compos. Struct. **164**, 130 (2017).
4. S.C. Pradhan, C.T. Loy, K.Y. Lam, J.N. Reddy, Appl. Acoust. **61**, 111 (2000).
5. Y.Q. Wang, Acta Astronaut. **143**, 263 (2018).
6. Y.Q. Wang, J.W. Zu, Aerospace Sci. Technol. **69**, 550 (2017).
7. H. Aminipour, M. Janghorban, L. Li, Compos. Struct. **190**, 91 (2018).
8. W. Zhang, Y.X. Hao, J. Yang, Compos. Struct. **94**, 1075 (2012).
9. H. Huang, Q. Han, Eur. J. Mech. A/Solids **29**, 42 (2010).
10. C.M. Craciunescu, M. Wuttig, J. Optoelectron. Adv. Mater. **5**, 139 (2003).
11. Y. Fu, H. Du, W. Huang, S. Zhang, M. Hu, Sensors Actuat. A **112**, 395 (2004).
12. Z. Lee, C. Ophus, L.M. Fischer, N. Nelson-Fitzpatrick, K.L. Westra, S. Evoy, V. Radmilovic, U. Dahmen, D. Mitlin, Nanotechnology **17**, 3063 (2006).
13. X. Li, B. Bhushan, K. Takashima, C.W. Baek, Y.K. Kim, Ultramicroscopy **97**, 481 (2003).
14. Y. Fu, H. Du, S. Zhang, Mater. Lett. **57**, 2995 (2003).
15. H.M. Sedighi, F. Daneshmand, M. Abadyan, Compos. Struct. **132**, 545 (2015).
16. A. Witvrouw, A. Mehta, Mater. Sci. Forum **492–493**, 255 (2005).
17. X.L. Jia, J. Yang, S. Kitipornchai, C.W. Lim, Appl. Math. Model. **36**, 1875 (2012).
18. M. Arefi, A.M. Zenkour, Mod. Phys. Lett. B **32**, 1 (2018).
19. K. Mohammadi, M. Mahinzare, K. Ghorbani, M. Ghadiri, Microsyst. Technol. **24**, 1133 (2017).
20. C.S. Zhu, X.Q. Fang, J.X. Liu, Int. J. Mech. Sci. **133**, 662 (2017).
21. S. Sahmani, M.M. Aghdam, Int. J. Mech. Sci. **131–132**, 95 (2017).
22. S. Sahmani, M.M. Aghdam, Compos. Struct. **178**, 97 (2017).
23. J. Sun, C.W. Lim, Z. Zhou, X. Xu, W. Sun, J. Appl. Phys. **119**, 214303 (2016).
24. M.H. Shojaeefard, H. Saeidi Googarchin, M. Mahinzare, M. Adibi, J. Intell. Mater. Syst. Struct. **29**, 2344 (2018).
25. H. Zeighampour, M. Shojaeian, J. Braz. Soc. Mech. Sci. Eng. **39**, 2789 (2017).
26. X.Q. Fang, C.S. Zhu, J.X. Liu, J. Zhao, Mater. Res. Express **5**, 45017 (2018).
27. Y.G. Hu, K.M. Liew, Q. Wang, X.Q. He, B.I. Yakobson, J. Mech. Phys. Solids **56**, 3475 (2008).
28. H. Zeighampour, Y.T. Beni, I. Karimipour, Microfluid. Nanofluid. **21**, 1 (2017).
29. H. Zeighampour, Y. Tadi Beni, M. Botshekanan Dehkordi, Thin-Walled Struct. **122**, 378 (2018).
30. L.H. Ma, L.L. Ke, J.N. Reddy, J. Yang, S. Kitipornchai, Y.S. Wang, Compos. Struct. **199**, 10 (2018).
31. Q. Wang, V.K. Varadan, Smart Mater. Struct. **16**, 178 (2007).
32. Y.S. Touloukian, *Thermophysical Properties of High Temperature Solid Materials* (Macmillian, New York, 1967).
33. W. Zhang, J. Yang, Y.X. Hao, Nonlinear Dyn. **59**, 619 (2010).
34. Y.Q. Wang, Y.H. Wan, J.W. Zu, Thin-Walled Struct. **135**, 537 (2019).
35. A.C. Eringen, *Nonlocal Polar Field Models* (Academic, New York, 1976).
36. A.C. Eringen, J. Appl. Phys. **54**, 4703 (1983).
37. W. Flügge, *Stresses in Shells* (1960).
38. J.N. Reddy, C.D. Chin, J. Therm. Stresses **21**, 593 (1998).
39. Y. Tadi Beni, F. Mehralian, H. Razavi, Compos. Struct. **120**, 65 (2015).
40. F. Mehralian, Y.T. Beni, Composites Part B **94**, 11 (2016).